Journal of Photochemistry and Photobiology A: Chemistry 222 (2011) 1–9

Contents lists available at ScienceDirect

Journal of Photochemistry and Photobiology A: Chemistry

journal homepage: www.elsevier.com/locate/jphotochem

UV-induced cyclization in myrcene isolated in rigid argon environment: FT-IR and DFT study

A. Kaczor[a,b,*], I. Reva[b], D. Warszycki[a], R. Fausto[b]

[a] Faculty of Chemistry, Jagiellonian University, Ingardena 3, 30-060 Krakow, Poland
[b] Department of Chemistry, University of Coimbra, P-3004-535 Coimbra, Portugal

ARTICLE INFO

Article history:
Received 29 December 2010
Received in revised form 7 February 2011
Accepted 10 February 2011
Available online 21 February 2011

Keywords:
Myrcene
Terpenes
Matrix isolation
Infrared spectroscopy
Photoisomerization
DFT calculations

ABSTRACT

The UV-induced photochemistry of monomeric myrcene [CH_2=C(R)–C(H)=CH_2, where R is –CH_2CH_2CH=$C(CH_3)_2$] isolated in a low-temperature argon matrix (13 K) was investigated by infrared spectroscopy and quantum-chemical calculations. Twenty-seven unique conformers of myrcene were predicted theoretically at both the DFT(B3LYP) and MP2 levels of approximation, with the 6-311++G(d,p) basis set. The most stable conformers were found to have the vinyl fragment in the *s-trans* orientation, and dominate in the equilibrium conformational mixture at room temperature. The experimental FTIR spectrum of the matrix-isolated compound was found to be well-reproduced by the superposition of the spectra of the three most stable forms of myrcene. These three forms differ structurally only by the arrangement of the vinyl groups relatively to the side chain. Narrowband selective as well as broadband UV irradiation of the matrix-isolated compound were found to lead to its cyclization to the cyclobutene-type product, 1-(4-methylpent-3-en-1-yl)cyclobutene. By analogy to butadiene, this photoprocess is proposed to result from accessing a conical intersection between the $\pi\sigma^*$ S_1 "dark" and S_0 states.

1. Introduction

Myrcene (β-myrcene, 7-methyl-3-methylene-1,6-octadiene) is an acyclic monoterpene of geranium odor occurring naturally in several essential oils derived from plants such as wormwood, bay leaf, ylang–ylang, wild thyme, jambu, juniper, lemongrass, *Zanthoxylum ovalifolium* [1], curcuma [2] or *Coleonema* [3]. Myrcene is industrially obtained by thermally induced β-pinene rearrangement [4,5] and is a starting material in the technological production of several important olefinic scents such as menthol, nerol, geraniol, citral, citronellal or citronellol [1]. Myrcene is also a substrate in one of the possible routes of vitamin E synthesis [6,7], and has also been tested, after hydrogenation, as a potential diesel fuel additive [8].

The synthesis of β-myrcene from β-pinene upon thermal treatment is an example of an isomerization reaction. Isomerization reactions are characteristic for terpenes, and have crucial biochemical and industrial consequences. Biochemically, *cis–trans* isomerization is the molecular fundamental step of the vision process, initiated by photoisomerization of 11-*cis*-retinal to its *all-trans* form. The 15-*cis* to *all-trans* isomerization proceeding *via* triplet state is related to the photoprotective function of the carotenoids [9]. It is considered that the long lifetime of the 90° configuration around the central double bond in these molecules is responsible for the antioxidant properties of β-carotenes [4,10,11]. Not only light, but also other stressing factors, such as heating or dissolving, may induce isomerization of terpenes [12], among which carotenoids (40 carbon atoms polyene compounds) attract particular attention as important nutrients in human diet. Extraction of carotenoids out of plants and further food processing (blanching, pasteurization, heating, canning) result frequently in their degradation or isomerization to *cis* isomers, that in general have lower bioavailability and antioxidant capacity [12–19]. Illustrative examples are the vitamin A precursors: 9-*cis* and 13-*cis*-β-carotene, with 38 and 53% activity, respectively, compared to the *all-trans* isomer [20].

Even for small terpenes, such as myrcene, thermally or photoinduced reactions can produce a variety of cyclic isomers, depending on the initiating factor and conditions of the reaction [21–27].

Thermal isomerization of β-pinene (**2**, in Scheme 1) results in formation of myrcene (**1**) as a main product, followed by reactions bringing five- and seven-membered-ring containing products (**5** and **6**) [27]. The photoinduced rearrangement yields different products, depending additionally on whether the reaction proceeds *via* singlet or triplet state [22–26]. According to Crowley [22,23],

* Corresponding author at: Faculty of Chemistry, Jagiellonian University, Ingardena 3, 30-060 Krakow, Poland. Tel.: +48 12 6632064.
E-mail address: kaczor@chemia.uj.edu.pl (A. Kaczor).

1010-6030/$ – see front matter © 2011 Elsevier B.V. All rights reserved.
doi:10.1016/j.jphotochem.2011.02.007

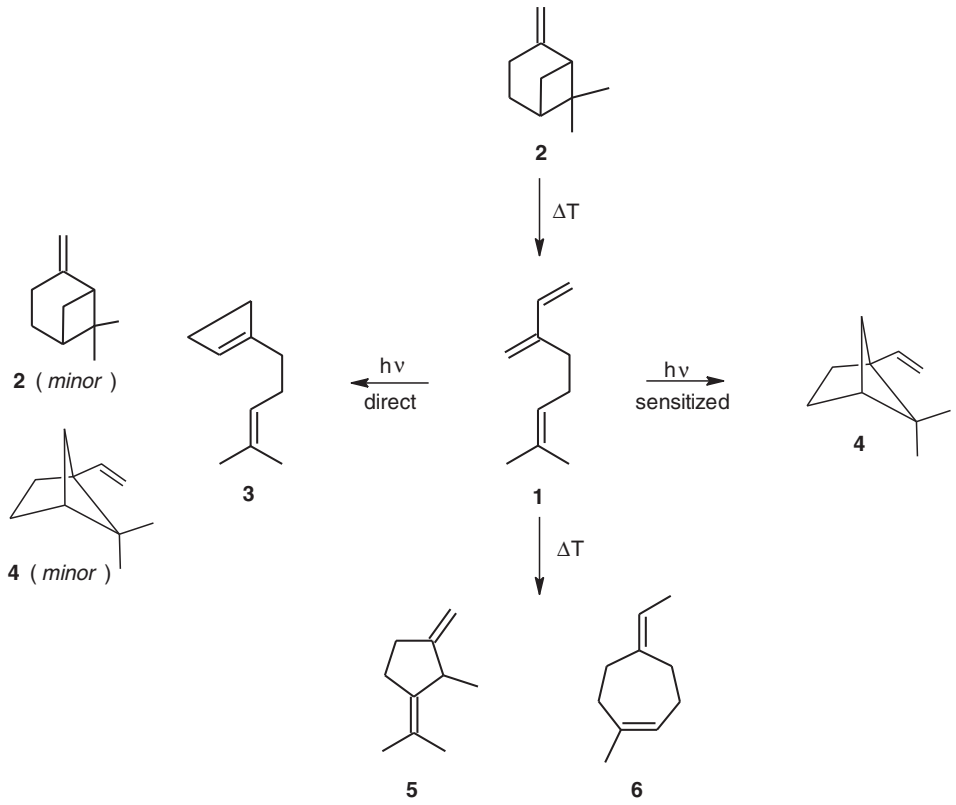

Scheme 1. Myrcene (**1**) and its photo- and thermoisomerization products: β-pinene (**2**); 1-(4-methylpent-3-en-1-yl)cyclobutene (**3**); 5,5-dimethyl-1-vinylbicyclo[2.1.1]hexane (**4**); 2-methyl-1-(1-methylethylidene)-3-methylidenecyclopentane (**5**); (5*E*)-5-ethylidene-1-methyl-cycloheptene (**6**).

direct irradiation of myrcene with UV light ($\lambda > 220$ nm) results in cyclization to 1-(4-methylpent-3-en-1-yl)cyclobutene (**3**; principal product) and β-pinene (minor product; *ca.* 10%), accompanied with unidentified products. Dauben et al. [24] obtained similar results, identifying 1-(4-methylpent-3-en-1-yl)cyclobutene as the main photoproduct together with a minor amount (less than 5%) of 5,5-dimethyl-1-vinylbicyclo [2.1.1]hexane (**4**); this latter compound, on the other hand, is the sole photoproduct of myrcene in the presence of photosensitizers, independently of the applied sensitizer and solvent [26].

Studying carotenes is a demanding task, both from computational and experimental perspectives. Hence, this work is part of our research program on isomerization of carotenes, in which small monoterpenes are treated as model compounds. Our main research aim is to reach general conclusions about the isomerization pathways for monoterpenes differing structurally, i.e. by side groups, length of hydrocarbon chain and its arrangement (cyclic, linear). The study of the isomerization processes in various environments, and particularly upon different stressing factors (light, temperature), is being developed to ultimately extrapolate the results to larger, more complex systems.

In this work, myrcene was isolated in a low temperature matrix and submitted to isomerization upon UV–vis irradiation. The structure of myrcene in the isolated phase is described and analyzed, while the emphasis is given to the photoisomerization of the compound taking place both under narrow and broadband irradiation.

2. Materials and methods

2.1. Experimental

Myrcene (β-myrcene, 7-methyl-3-methylene-1,6-octadiene, ≥95.0%) was obtained from Fluka.

In the matrix isolation experiments, a glass vacuum system and standard manometric procedures were used to deposit the matrix gas (argon, N60, obtained from Air Liquide). Matrices were prepared by co-deposition, onto the cooled CsI substrate of the cryostat, of the matrix gas (argon), and of the compound evaporated from a glass sample compartment connected to the cryostat *via* a needle valve, as described in Ref. [28]. During deposition, the sample compartment was cooled to 0 °C, while the valve nozzle was kept at room temperature (RT). This latter temperature then defined the equilibrium conformational composition of the myrcene vapors being deposited.

The IR spectra were collected, with 0.5 cm^{-1} spectral resolution, on a Nicolet 3600 Fourier Transform infrared spectrometer, equipped with a deuterated triglycine sulphate (DTGS) detector and a Ge/KBr beamsplitter.

All experiments were done on the basis of an APD Cryogenics closed cycle helium refrigeration system with a DE-202A expander [28]. The temperature of the CsI substrate during deposition was 13–14 K. Necessary modifications of the sample compartment of the spectrometer were made in order to accommodate the cryostat head and allow efficient purging of the instrument by a stream of dry air to remove water and CO_2 vapors.

The UV irradiation was carried out with pulsed narrowband UV radiation in the 240–271 nm range. It was generated by the third harmonic of a Nd-YAG Quanta-Ray PRO-230-10 pump laser (355 nm) and converted to the used UV frequency output (FWHM ~0.2 cm^{-1}) by an optical parametric oscillator (Spectra-Physics MOPO SL, with IEE-488 and MAP-SL options), coupled with a frequency doubling module FDO-970. The output pulses, having energy up to 2 mJ and repetition rate of 10 Hz, were directed to the sample via an external quartz window of the cryostat. Alternatively, the matrices were irradiated through the outer KBr or quartz window of the cryostat with light from a 500 W Hg(Xe) lamp

(Spectra-Physics, Model 66142), adjusted to provide 200 W output power.

In the course of the experiments, the temperature of the matrices was measured directly at the sample holder by a silicon diode sensor connected to a digital controller (Scientific Instruments, Model 9650-1) and did not exceed 14 K.

2.2. Computational

The quantum chemical calculations were performed with Gaussian 03 (Revision E.01) [29] or Gaussian 09 (Revision A1) [30] at the DFT level of theory, using the 6-311++G(d,p) basis set. The structures of myrcene conformers were additionally optimized at the MP2 level with the same basis set. The DFT calculations were carried out with the three-parameter density functional abbreviated as B3LYP, which includes Becke's gradient exchange correction [31] and the Lee, Yang and Parr correlation functional [32].

Vibrational frequencies were calculated at the same levels of theory as those used in the optimization of geometries, and the nature of the stationary points on the potential energy surface (PES) resulting from optimization was determined by inspection of the corresponding calculated Hessian matrix. The optimized structures of myrcene conformers and those of the studied photoproducts were confirmed to correspond to true minimum energy conformations on the PES. Potential energy profiles for internal rotations were calculated performing a relaxed scan on the PES along the relevant reaction coordinates, and the transition state structures for conformational interconversions were obtained using the Synchronous Transit-Guided Quasi-Newton (STQN) method [33,34]. Vertical excitations were calculated using the time-dependent DFT (TD-DFT) method [35,36].

The calculated harmonic frequencies were used in the analysis of the experimental spectra. They were scaled down, to account mainly for anharmonicity effects and limitations of the basis set. The scaling factors for the CH stretching (0.960) [37] and the fingerprint (0.980) [38–40] regions of spectra were adopted from the previous works comparing the experimentally observed bands of matrix isolated compounds with the harmonic vibrational frequencies calculated at the B3LYP/6-311++G(d,p) theory level, the same as used in the present work.

Potential energy distributions (PED) of the normal modes were computed in terms of natural internal coordinates [41] with the GAR2PED program [42].

3. Results and discussion

3.1. Theoretical calculations

Fig. 1 shows the structure of myrcene with the numbering scheme adopted in this study. The conformational multiplicity of the molecule is defined by four degrees of freedom, namely rotations around the C_2–C_{12}, C_{12}–C_{15}, C_{15}–C_{18} and C_{18}–C_{22} internal axes.

The maximum possible symmetry of myrcene molecule is the C_s point group. Any structure deviating from the C_s symmetry will belong to the C_1 point group, and will have a mirror-image conformer with all dihedral angles having the opposite signs. It happens that any of the C_s arrangements requires C_1=C_2–C_{12}–C_{15} dihedral angle to adopt one of the two values: either 0° or 180°. Rotation around the C_2–C_{12} bond results in a crowded geometry and absence of a minimum for the C_1=C_2–C_{12}–C_{15} dihedral angle around 0° (*cis* orientation). The 180° (*trans*) alternative is not related with any crowded geometry but no minimum geometry could be located around this value either. The minimum energy conformations around this bond were found only for two

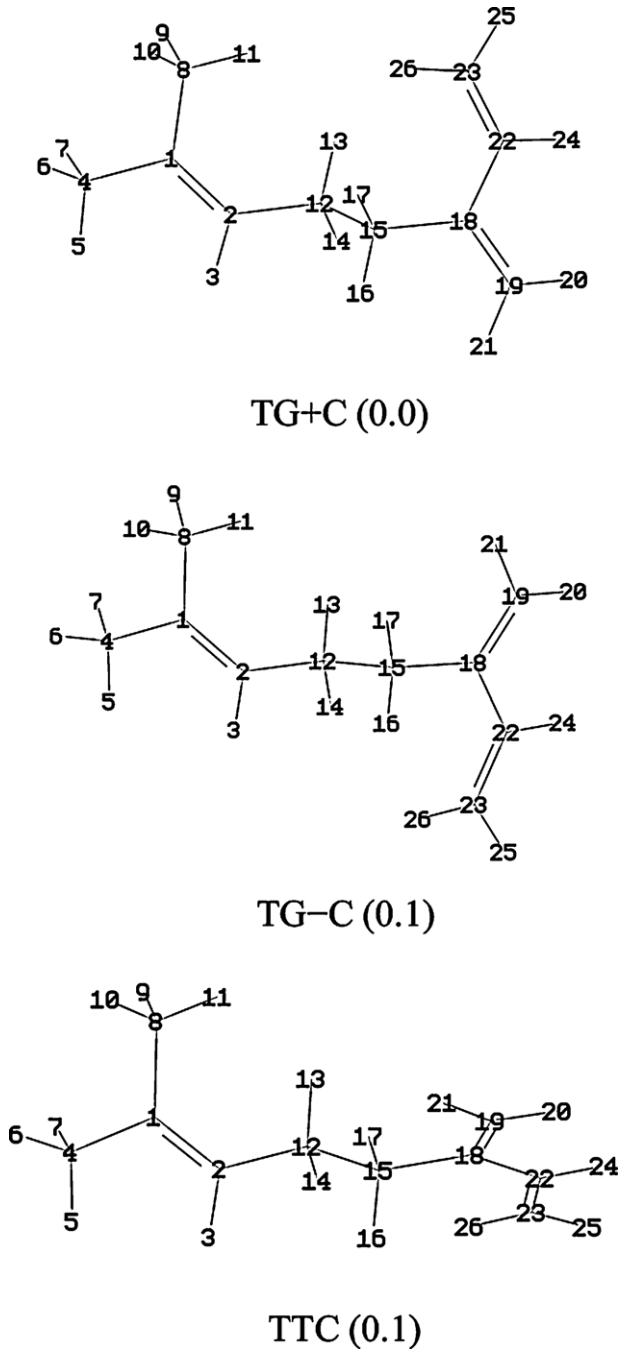

Fig. 1. Optimized (B3LYP/6-311++G(d,p)) geometry of the three most stable conformers of myrcene with the numbering scheme. Zero-point corrected energy (in kJ mol^{-1}) relative to the most stable *TG+C* form is given in parenthesis.

equivalent-by-symmetry values of the C_1=C_2–C_{12}–C_{15} dihedral angle: around *ca.* +120° and *ca.* −120°. Therefore, the whole set of conformers of myrcene of C_1 symmetry can be divided in two groups, each one corresponding to a specific orientation of the C_1=C_2–C_{12}–C_{15} dihedral (*ca.* +120° or *ca.* −120°). In this work, only the set of structures for which internal rotation around the C_1=C_2–C_{12}–C_{15} axis results in the *skew*+ arrangement (*ca.* +120°) will be considered, as the *skew*− forms are mirror images of the former. All unique conformers are then characterized by a specific combination of arrangements around C_{12}–C_{15}, C_{15}–C_{18} and C_{18}–C_{22}. The internal rotation around these three torsional coordinates resulted in twenty seven conformers, which are described in Table 1 according to the B3LYP/6-311++G(d,p) calculations.

Table 1
Relative zero-point corrected energies (ΔE_{corr}, in kJ mol^{-1}), Gibbs free energies at 298.15 K (ΔG, in kJ mol^{-1}), abundances at 298.15 K (A_{calc}, in %) and values of torsion angles (in degree) of myrcene conformers calculated at the B3LYP/6-311++G(d,p) level of theory.

Conformer[a]	ΔE_{corr}[b]	ΔG[c]	A_{calc}[d]	C_2–C_{12}–C_{15}–C_{18}	C_{12}–C_{15}–C_{18}–C_{22}	C_{15}–C_{18}–C_{22}=C_{23}
TG+C	0.0	0.0	25.4	178.8	79.1	4.6
TG−C	0.1	0.3	22.5	176.1	−78.0	−5.0
TTC	0.1	0.1	24.4	177.0	−179.5	0.0
G−G−C	3.2	4.7	3.8	−72.3	−77.2	−4.2
G+G+C	3.5	4.5	4.1	66.0	76.2	4.5
G−TC	5.0	5.7	2.6	−71.0	177.9	−0.5
G+TC	5.9	3.2	7.0	72.8	−172.8	0.3
TG−Sk+	7.3	6.3	2.0	176.2	−67.2	143.6
TG+Sk−	7.5	6.7	1.7	178.6	68.0	−143.3
G+Sk−C	7.7	8.6	0.8	64.6	−96.5	−0.3
G−Sk+C	8.5	9.0	0.7	−68.4	99.0	3.0
TG−Sk−	9.5	8.4	0.9	175.7	−75.3	−146.0
TG+Sk+	9.8	7.8	1.1	178.2	76.5	146.5
TTSk+	9.9	9.1	0.6	177.7	178.3	142.6
TTSk−	9.9	10.0	0.5	176.7	−178.2	−141.8
G+G+Sk−	10.3	9.8	0.5	65.1	64.5	−144.0
G−G−Sk+	10.7	9.8	0.5	−70.4	−68.0	144.2
G+G+Sk+	12.8	11.9	0.2	64.8	71.6	145.7
G−G−Sk−	13.4	13.7	0.1	−72.4	−75.7	−147.3
G−G+Sk−	14.2	13.7	0.1	−75.4	72.5	−148.3
G−G+Sk+	14.4	14.2	<0.1	−72.1	84.6	143.0
G−TSk+	14.8	14.0	0.1	−70.4	176.2	141.0
G−TSk−	15.1	15.3	<0.1	−71.4	179.3	−143.2
G+G−Sk+	15.1	13.8	0.1	66.8	−78.7	147.9
G+TSk−	15.5	14.4	<0.1	71.4	−168.6	−139.6
G+Sk−Sk−	15.7	15.0	<0.1	60.5	−93.2	−145.8
G+TSk+	15.8	14.5	<0.1	72.5	−172.7	143.9

[a] B3LYP/6-311++G(d,p); all structures have C_1 symmetry.
[b] E_{corr} = −390.528868 Hartree for conformer *TG+C*.
[c] *G* = −390.568206 Hartree for conformer *TG+C* at 298.15 K.

The following scheme was applied to the conformer naming: the first letter denotes the conformation in respect to the C_2–C_{12}–C_{15}–C_{18} dihedral, while the second and the third positions (one- or two-letter abbreviations) designate the arrangements around the C_{12}–C_{15}–C_{18}–C_{22} and C_{15}–C_{18}–C_{22}=C_{23} angles, respectively. *C*, *G+*, *G−*, *Sk+*, *Sk−* and *T* denote *cis* (*ca.* 0°), *gauche+* [30°/90°], *gauche−* [−30°/−90°], *skew+* [90°/150°], *skew−* [−90/−150°] and *trans* (*ca.* 180°) arrangements, respectively.

According to the DFT calculations, the three most stable forms have *trans* and *cis* conformations around the C_2–C_{12}–C_{15}–C_{18} and C_{15}–C_{18}–C_{22}=C_{23} torsional angles, respectively, while differing in the arrangement around the C_{12}–C_{15}–C_{18}–C_{22} dihedral angle. These conformers are predicted to be almost isoenergetic and constitute above 72% of the estimated population of myrcene at 298.15 K (RT). The seven most stable forms constitute about 90% of the equilibrium population at RT, according to the DFT prediction. It is important to note that in these dominating seven forms the vinyl group (i.e. the C_{19}=C_{18}–C_{22}=C_{23} moiety) adopts the *s-trans* orientation.

Internal rotation around C_{18}–C_{22}: A particularly important factor deciding on the relative energies of myrcene conformers is the arrangement of the C_{15}–C_{18}–C_{22}=C_{23} fragment. The *cis* arrangement of the C_{15}–C_{18}–C_{22}=C_{23} angle, found in the seven most stable minima of the compound, imposes the s-*trans* conformation of the vinyl groups (i.e., of the C_{19}=C_{18}–C_{22}=C_{23} fragment). The energetic preference of *s-trans* over the more strained *s-gauche* conformation in 1,3-butadiene was computationally predicted to amount to 11.2–16.9 kJ mol^{-1}, depending on the level of theory applied [43], which is in agreement with experimentally obtained values of 10.5 [44] and 11.8 kJ mol^{-1} [45]. In myrcene, the energy differences between conformers differing only by the arrangement of the vinyl group (for example *TG+C* versus *TG+Sk+* or *TG+Sk−*) were predicted to be slightly lower (6.8–10.2 kJ mol^{-1}), though still being the most important factor determining the relative energy of the conformers.

Internal rotation around C_{15}–C_{18}: On the contrary, the conformation around the C_{15}–C_{18} bond practically does not influence the energy of the three most stable myrcene conformers. Indeed, in general the energy difference between conformers of myrcene differing only by the value of this angle is not larger than 5.4 kJ mol^{-1} (*G+G+Sk−* versus *G+Sk−Sk−*), and in most cases does not exceed 3 kJ mol^{-1}. Additionally, no energetic preference for any particular conformation (*gauche+*, *gauche−* or *trans*) was noticed.

Internal rotation around C_{12}–C_{15}: Finally, regarding the geometry around the C_{12}–C_{15} bond, the calculations indicate that the *trans* arrangement of C_2–C_{12}–C_{15}–C_{18} dihedral is energetically favored (about 2.8–7.8 kJ mol^{-1}) over the *gauche* in the whole set of conformers.

Previously, based on spectroscopic matrix-isolation studies of five isomeric butane-diols, it was shown that the MP2 method could reliably simulate the relative energies of butane-diol conformers [46–49]. Butane-diols exhibit a high degree of conformational freedom, similarly to myrcene. Therefore, the structures of myrcene conformers were also optimized at the MP2 level (see Table S1, Supplementary Material). The energies, and hence the populations of myrcene conformers, obtained at the MP2 level, differ somewhat from those predicted by the DFT computations. One of the main differences is that the relative conformational energies are more evenly distributed over the energy scale. There is not a well-defined energy gap between the stabilities of the three most stable structures and the remaining conformers. The main similarity between the DFT and MP2 calculations is that the *s-trans* orientation of the vinyl fragment dominates among the most stable forms. The seven most stable conformers, according to the MP2 calculated Gibbs energies, constitute above 82% of the equilibrium population of myrcene at 298.15 K.

Noteworthy, the MP2-calculated infrared spectra of almost all forms are similar, so that identification of the particular conformers based on this method is practically impossible. This is also true for the DFT calculations. This result is not surprising. Due to the struc-

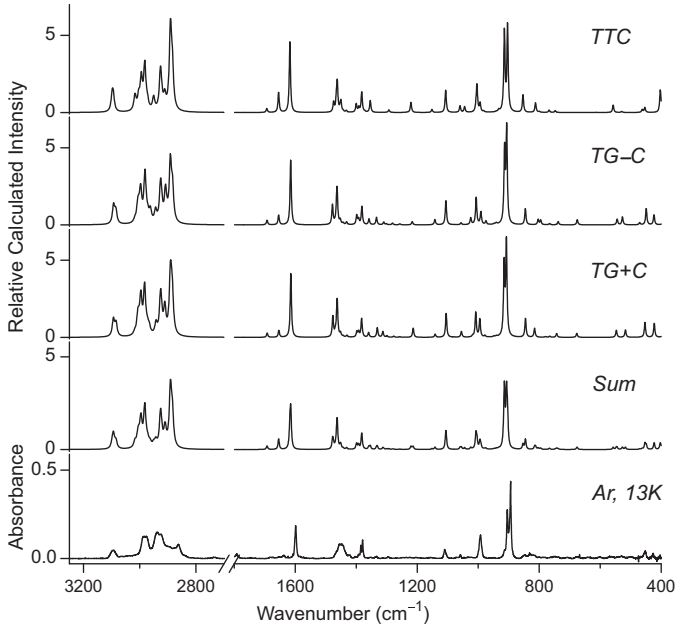

Fig. 2. Experimental FT-IR spectrum of matrix-isolated myrcene (Ar, 13 K), compared with the theoretical spectra of the three most stable myrcene conformers (*TG+C*, *TG−C* and *TTC*) and the sum spectrum (Sum) obtained by adding the population-weighted spectra of these conformers (see Table 1). Theoretical spectra have been broadened by Lorentzian profiles having FWHM of 10 cm^{-1} (CH stretching range) and 5 cm^{-1} (fingerprint range) and centered at the calculated frequencies scaled by 0.960 and 0.980, respectively.

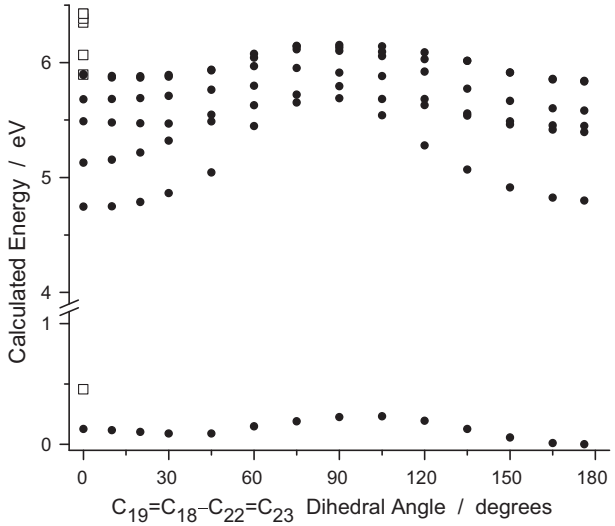

Fig. 3. TD-DFT profiles of the six lowest energy singlet states of myrcene calculated at the B3LYP/6-311++G(d,p) level of theory as functions of the internal rotation of the C_{19}=C_{18}–C_{22}=C_{23} dihedral angle, starting from conformer *TG+C* (around 180°). Open squares at 0° correspond to the lowest energy singlet states of 1-(4-methylpent-3-en-1-yl)cyclobutene, where atoms C_{19}–C_{18}=C_{22}–C_{23} form a closed ring. Note the ordinate break.

ture of the compound (lack of electron lone pairs, strong electron donors or acceptors) the similarity of the vibrational signatures due to different conformers is expectable. Nevertheless, comparison of the experimental FTIR spectra of matrix-isolated myrcene with the theoretical infrared spectra calculated at the DFT and MP2 levels indicates that the DFT method reproduces the experimental data better. Therefore, this method was chosen to model the obtained experimental spectroscopic results.

3.2. Matrix-isolated myrcene

The predicted values of interconversion barriers between the three most stable forms are: *ca.* 31 kJ mol^{-1} for *TG−C* rotamerization to *TG+C*, and *ca.* 7 kJ mol^{-1} for rotamerization of *TTC* both into *TG−C* or *TG+C*. The value of the first barrier is considerably higher as the transition state requires the C_{12}–C_{15}–C_{18}–C_{22} dihedral in the nearly *cis* arrangement and repulsive interactions between H_{26} and C_{12} methylene protons. The energies for the conformational isomerization among the above forms calculated at the MP2 level of theory were found to be even higher than the DFT calculated values. Therefore, all predicted barriers can be considered too high to be overcome during matrix deposition and we can expect the *TTC*, *TG−C* and *TG+C* to contribute to the observed spectrum of the as-deposited matrix in the ratio of their populations in gas phase prior to deposition. Then, on the whole these forms shall account for at least 72% of the total spectrum intensity (it is possible that some of the higher energy forms might have low energy barriers of conversion into the most stable forms and convert to them during deposition). All the other forms could be expected to have individual contributions much smaller that those of the three most stable conformers.

The experimental FT-IR spectrum of myrcene isolated in solid argon at 13 K is presented in Fig. 2, along with the computed spectra of the *TG+C*, *TG−C* and *TTC* conformers of the compound and the sum spectrum obtained by adding the spectra of these conformers after multiplying them by the abundance factors at 298.15 K (namely 0.254, 0.225 and 0.244, respectively; see Table 1), which at a good approximation fits nicely the experimental spectrum. Fig. 2 shows also that, as it was mentioned above, there are no striking differences in the spectra of the most stable conformers. Also as it could be anticipated, accounting for the theoretical spectra of other minima does not influence the shape of the simulated spectrum either, as their abundances are small.

Apart from the CH stretching region, where bands are overlapped and difficult to analyze, the most intense spectral features in the spectrum of myrcene are observed at 894, 904, 905, *ca.* 992, 1379, 1385 and 1599 cm^{-1} and in the 1430–1500 cm^{-1} range. Bands at 894, 904 and 905 cm^{-1} are assigned to out-of-plane wagging vibrations of the $C_{19}H_{21}$ fragment (calc: 904, 907, 908 cm^{-1}, for *TTC*, *TG−C* and *TG+C* conformers, respectively). In case of these, but also for other less intense spectral features, a tentative assignment was made to individual conformers (see Tables S3–S4, Supplementary Material). Very unfortunately, the bands associated with the C_{12}–C_{15} stretching vibration, although predicted at quite different frequency for *gauche* and *TTC* forms (991, 995 and 1007 cm^{-1} for *TG−C*, *TG+C* and *TTC*, respectively), cannot be identified in the spectra as they are superimposed by the more intense band due to the C_1–C_4–$H_{5,6,7}$ rocking and C_{22}–C_{23} torsional vibrations, therefore contributing altogether to the quite broad structured band in the experimental spectrum centered at *ca.* 992 cm^{-1}. The bands observed at 1379 and 1385 cm^{-1} are attributed to the symmetric bending modes of the two methyl groups (at C_4 and C_8) in antiphase, while those in the 1430–1500 cm^{-1} range are connected mostly with the asymmetric CH_3 bending vibrations and $C_{12}H_{13,14}$ and $C_{15}H_{16,17}$ scissoring modes. The band centered at 1599 cm^{-1} is assigned to the antisymmetric stretching vibration of the C_{18}=C_{19} and C_{22}=C_{23} bonds. The proposed assignment of other spectral features of weak intensity is given in Tables S3–S4 (Supplementary Material).

3.3. Photochemistry of matrix-isolated myrcene

The structure of myrcene incorporates three double bonds, two of them conjugated (C_{22}=C_{23} and C_{19}=C_{18}) and the third (C_1=C_2) separated from the latter by two methylene groups. An adequate

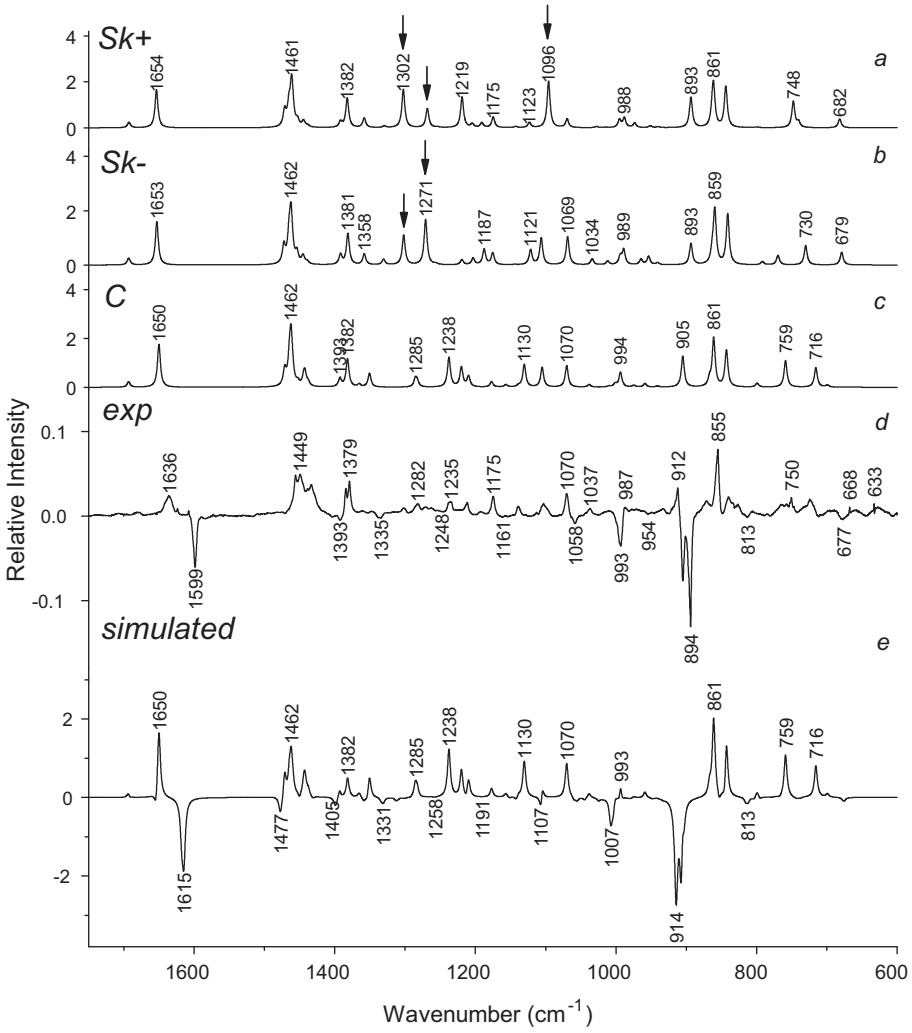

Fig. 4. Theoretical spectra of MCB conformers (a–c), FT-IR spectrum obtained by subtraction of the spectrum due to matrix-isolated myrcene (Ar, 13 K) from the spectrum after irradiation with 240, 235 and 230 nm light (for 60, 20 and 10 min, respectively) (d), and theoretical difference spectrum: spectrum of the RT equilibrium mixture of the three myrcene conformers minus spectrum of *cis* MCB (in a 1:0.7 ratio obtained as the best fit to the experiment). (e) Theoretical spectra have been broadened by a Lorentzian having a width of 5 cm^{-1}; arrows in the theoretical spectra point to intense bands of the skew MCB conformers whose expected counterparts are absent or very weak in the experimental spectrum.

model molecule to understand the photochemistry of myrcene is buta-1,3-diene (for simplicity, butadiene, thereafter), as myrcene can be treated as butadiene in which a methine proton is replaced by the CH_2–CH_2–CH=C–$(CH_3)_2$ fragment. Upon irradiation with UV-light (λ = 254 nm), butadiene (5% in cyclohexane) undergoes isomerization to cyclobutene (a major product) and bicyclo [1.1.0]-butane [50]. Butadiene exists in two conformations: *s-trans* (the most stable form) and *s-gauche* (also called *s-cis*), the latter being *ca.* 10–17 kJ mol^{-1} higher in energy than *s-trans* [43]. Matrix-isolated *s-trans*-butadiene was demonstrated to undergo isomerization to the less stable form upon 214 nm irradiation (zinc lamp) [50]. The reaction was reversible upon irradiation with a high-pressure mercury-xenon lamp (which has low light intensity for λ < 230 nm), and the produced s-*trans* butadiene was found not to isomerize into cyclobutene, nor to bicyclobutane (only vinylacetylene was formed on prolonged irradiation) [51].

A very fast (approximately 35 fs lifetime) decay from the absorbing (ionic) state $1B_u$ state to the covalent $2A_g$ state was found in the course of the photoreaction of *s-trans*-butadiene [52], in agreement with the computed CASPT2 value of *ca.* 30–40 fs [53]. The very short lifetime of the $1B_u$ state rationalizes the lack of fluorescence of the compound [54]. Mechanistically, the excited-state $1A_g$ reaction pathways were explained in detail for *s-cis* butadiene and some substituted butadienes (namely 2,3-dimethylbutadiene and 2-cyanobutadiene) [55–58]. The ring-closure mechanism proceeds disrotatory *via* the $1B_u/2A_g$ conical intersection (CI) located near the C_s equilibrium structure and evolves toward the $2A_g/1A_g$ CI that is a branching point leading to cyclobutene, bicyclobutane or *s-trans* butadiene isomers [55,57].

In line with previous findings, our TD-DFT/6-311++G(d,p) computations predict that the first excited singlet state of myrcene (S_1) is dark (258 nm, f = 0.0177; 259 nm, f = 0.0322 and 253 nm, f = 0.0025 for *TG+C*, *TG−C* and *TTC* forms, respectively). For *TG+C*, the state of high oscillator strength (f = 0.4119) is S_2, computed at 230 nm. For the other experimentally relevant conformers of myrcene, the highest oscillator strength state is S_3 and is predicted at 228 nm (f = 0.4032) and 226 nm (f = 0.4105), for *TG−C* and *TTC*, respectively. These states might be related to the 225 nm absorption band in the UV–vis spectrum of myrcene (ε_{max} 15,350) [59]. By analogy with other polyenes, it is assumed that the "bright" S_2 (or S_3) state has a very short lifetime and the photoreaction proceeds in the S_1 "dark" state (after excitation to S_2 or S_3).

The energies of the lowest singlet states of myrcene are represented graphically in Fig. 3. To obtain these energies, all geometrical parameters except for the dihedral angle were optimized so that the energy of S_0 state becomes a minimum, and then the ver-

tical excitation energies were calculated at every value of the C_{19}=C_{18}–C_{22}=C_{23} dihedral angle. A clear ordering of the excited states is not easy. At the geometries corresponding to the minima on the S_0 surface (around 45° and 180°), the "dark" $\pi\sigma^*$ S_1 state has calculated energies of about 4.8 eV. At the same geometries, the "bright" $\pi\pi^*$ state has a vertical excitation energy of about 5.4–5.5 eV, which is very similar for the second and third excited singlet states. If myrcene undergoes the same photochemistry as butadiene does, and the starting points correspond to the most stable conformers, it should require an internal rotation around the C_{18}–C_{22} bond, and crossing the region where the C_{19}=C_{18}–C_{22}=C_{23} dihedral angle adopts values of about 90°. At such geometry, the first three excited states (S_1, S_2 and S_3) fall into a narrow energy range 5.5–5.7 eV (see Fig. 3), and their relative energy order changes. This change can be followed by monitoring the calculated oscillator strengths. In other words, the myrcene molecules excited to S_2 or S_3 $\pi\pi^*$ state, can easily move to the $\pi\sigma^*$ S_1 surface.

Fig. 4 presents the changes in the spectrum of matrix-isolated myrcene upon irradiation with the 240 nm laser light for 60 min and further with the 235 and 230 nm light for 20 and 10 min, respectively. As the progress of irradiation with the 240 nm light shows (see Fig. 5), the reaction follows a first order kinetics, and after 60 min of irradiation, approaches a plateau, i.e., a photostationary equilibrium is attained. At that point, a substantial amount of myrcene is still present. The distributions of bands appearing upon irradiation at 240, 235 and 230 nm are similar, although the ratios of increase of their relative intensities are different, showing that the kinetics of the photoreaction is significantly wavelength-dependent and that the reaction yield increases with the decrease of the laser wavelength toward the absorption maximum of myrcene (at 225 nm) [59].

The sole product of the photoreaction induced by irradiation with UV light within the λ = 230–240 nm range was identified as 1-(4-methylpent-3-en-1-yl)cyclobutene (called MCB hereafter). No other possible products such as β-pinene, 5,5-dimethyl-1-vinylbicyclo [2.1.1] hexane, 2-methyl-1-(1-methylethylidene)-3-methylidenecyclopentane and (5E)-5-ethylidene-1-methylcycloheptene (see Scheme 1), or photoproducts resulting from (*s-trans*) → (*s-cis)* isomerization were observed. Prolonged irradiation at 250 and 270 nm (for additional 25 and 15 min, respectively) did not lead to any additional products either. Furthermore, no other products could be found upon broadband irradiation of myrcene (Hg/Xe lamp). In the latter case, the photoproduct formation was just significantly slower. In particular, similar product: substrate ratios were obtained upon broadband irradiation for 180 min (200 W Hg(Xe) lamp, defocused, through a quartz window) and for 60 min irradiation with 240 nm laser light.

MCB has a reduced conformational freedom compared to myrcene. Additionally, rotation around the C_2–C_{12} and C_{12}–C_{15} bonds should be hindered due to rigidity of the matrix environment. Nonetheless, three conformers were computationally predicted resulting from rotation around the C_{15}–C_{18} bond, with *skew*+, *cis* (global minimum) and *skew*− arrangement of the C_{12}–C_{15}–C_{18}–C_{22} dihedral. As Fig. S1 (Supplementary Materials) demonstrates, the predicted energy barriers between *skew* forms and the *cis* conformer are *ca.* 7 kJ mol^{-1}. Taking into account this value, it seems probable that vibrationally "hot" molecules produced as the result of $S_1 \rightarrow S_0$ conversion can surpass the barriers. Therefore, only *cis* conformer was used to assign bands in the spectrum of irradiated myrcene, in agreement with the slightly better agreement of the theoretical spectrum of this conformer with the experimental data, compared to the spectra of the *skew* forms (particularly lack of intense bands at *ca.* 1100 and 1300 cm^{-1} in the latter denoted by arrows in Fig. 4).

The obtained product in order to be formed requires significant rearrangement of the C=C–C=C fragment of the molecule. Accord-

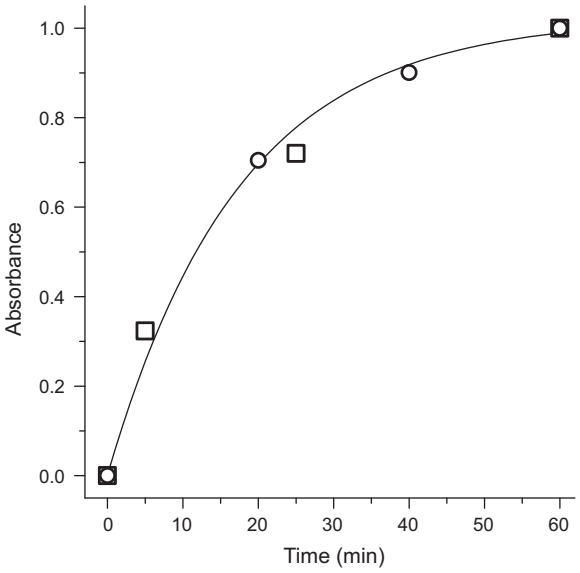

Fig. 5. Change with time of irradiation (laser light, λ = 240 nm) of the observed photoproduct of matrix-isolated myrcene. Circles: average of four well-defined bands (at 855, 1070, 1175 and 1237 cm^{-1}). Squares: data for the strongest band (855 cm^{-1}) from a separate experiment. The integrated experimental intensities were reduced by the calculated infrared intensity of the respective vibration. The reduced intensity after 1 h of irradiation was normalized to unity. Solid line is described by the equation: $y = 1 - \exp(-x/t_1)$, where t_1 = 17.5 min.

ing to Olivucci et al. [58] there are three $2A_g/1A_g$ CIs that are minima on the $2A_g$ potential energy surface of butadiene. The path from the *s-trans* minimum to the *s-transoid* CI is barrierless, while the *s-cis* to the *s-cisoid* CI pathway reaches *ca.* 16 kJ mol^{-1} above the minima [58]. Both pathways require the central C–C rotation and disrotatory motion of the methylene groups [58]. By analogy, for myrcene, the photoreaction leading to formation of MCB should proceed with the partial rotation of the central C–C bond and further formation of the four-membered product resulting from steeping the pathway *via* $2A_g/1A_g$ CI. Nevertheless, for myrcene, no other products that might result from accessing the S_1/S_0 *transoid* or *cisoid* CI, particularly *s-cis* C=C–C=C isomers, were observed experimentally. A similar situation was observed before for products of α-pyrone photoisomerization of the aldehyde-ketene type in low-temperature matrices [60]. The presence of the sole *s-trans* isomers in the matrix was explained by possible higher efficiency of the *s-cis* → *s-trans* photoprocess relative to the opposite one [60].

The kinetics of UV-induced formation of MCB suggests that this molecule accumulates in the matrix and does not react further. An explanation for this behaviour could be found in the results of TD-DFT calculations. The lowest energy excited states of MCB are presented in Fig. 3 as open squares. The calculated energies of the excited MCB singlet states are considerably higher than those of myrcene, being energetically inaccessible with the irradiation wavelengths used (as the highest-energy UV-light of our laser equipment equals to 220 nm). In addition, the calculated oscillator strengths of the first excited singlet states are extremely low: 0.0020; 0.0000; 0.0163; 0.0046; 0.0072, from S_1 to S_5, respectively. Therefore, the photoproduced MCB, under the present experimental conditions is unlikely to undergo UV-excitation.

4. Conclusions

The conformational multiplicity of myrcene is defined by three degrees of freedom, namely rotations around the C_{12}–C_{15}, C_{15}–C_{18} and C_{18}–C_{22} internal axes. All conformers belong to the C_1 point group. Three major conformers were predicted by the calculations

to be significantly populated in the gas phase at room temperature, having *trans* and *cis* conformations around the C_2–C_{12}–C_{15}–C_{18} and C_{15}–C_{18}–C_{22}=C_{23} torsional angles, respectively, while differing by the arrangement around the C_{15}–C_{18} bond. The observed IR spectrum of the matrix-isolated compound correlates well with the theoretical predictions. It matches a simulated spectrum composed from the calculated spectra of the three lowest energy conformers of myrcene scaled by their expected relative populations in the gas phase before matrix deposition. This result is also in agreement with the predicted values for the barriers for conformational isomerization, which were found to be high enough to be overcome during matrix deposition.

Upon excitation of matrix-isolated myrcene with either narrowband (laser) or broadband UV light, the molecule isomerized to a cyclobutene-type product, namely 1-(4-methylpent-3-en-1-yl)cyclobutene (MCB), which was the sole product observed. Three conformers were computationally predicted for MCB, with *skew*+, *cis* (global minimum) and *skew*− arrangement of the C_{12}–C_{15}–C_{18}=C_{22} dihedral. However, as the predicted barriers for internal rotation around the C_{15}–C_{18} bond in this molecule are low, and the theoretical IR spectrum of the *cis* form agrees better than those of the *skew* forms with the experimentally observed data, it seems most probable that the latter two conformers once produced in a vibrationally excited state relax to the *cis* form during the $S_1 \rightarrow S_0$ conversion. By analogy with butadiene, and taking into account the significant "mixing" of several lowest singlet excited states, the photochemical formation of MCB from myrcene is proposed to result from excitation of the molecule to either S_2 or S_3 $\pi\pi^*$ states, followed by fast relaxation to the $\pi\sigma^*$ S_1 surface and further relaxation to the ground state through one of the S_1/S_0 CIs on the singlet potential energy manifold of myrcene. The kinetics of UV-induced formation of MCB suggests that this molecule accumulates in the matrix and does not react further, a result that agrees with TD-DFT calculations, which predict that the excited MCB singlet states are considerably higher in energy than those of myrcene and possess very small oscillator strengths.

Acknowledgements

This work was supported by the Polish Ministry of Science and Higher Education (Grant No. 204311037, 2009–2012) and the Portuguese Science Foundation (FCT, Project PTDC/QUI-QUI/111879/2009, also supported by QREN – FEDER/COMPETE). Academic Computer Centre Cyfronet is acknowledged for CPU time.

Appendix A. Supplementary data

Supplementary data associated with this article can be found, in the online version, at doi:10.1016/j.jphotochem.2011.02.007.

References

[1] A. Behr, L. Johnen, Myrcene as a natural base chemical in sustainable chemistry: a critical review, ChemSusChem 2 (2009) 1072.
[2] S. Behura, V.K. Srivastava, Essential oils of leaves of Curcuma species, J. Essent. Oil Res. 16 (2004) 109.
[3] K.H.C. Baser, B. Demirci, T. Ozek, A.M. Viljoen, J.E. Victor, Composition of the essential oils of five Coleonema species from South Africa, J. Essent. Oil Res. 18 (2006) 26.
[4] W.E. Doering, T. Kitagawa, Thermal *cis–trans* rearrangement of semirigid polyenes as a model for the anticarcinogen beta-carotene: an all-trans-pentaene and an all-trans-heptaene, J. Am. Chem. Soc. 113 (1991) 4288.
[5] L.A. Goldblatt, S. Palkin, US 2,420,131, 1947.
[6] W. Bonrath, M. Eggersdorfer, T. Netscher, Catalysis in the industrial preparation of vitamins and nutraceuticals, Catal. Today 121 (2007) 45.
[7] W. Bonrath, T. Netscher, Catalytic processes in vitamins synthesis and production, Appl. Catal. A Gen. 280 (2005) 55.
[8] N.I. Tracy, D.C. Chen, D.W. Crunkleton, G.L. Price, Hydrogenated monoterpenes as diesel fuel additives, Fuel 88 (2009) 2238.
[9] Y. Koyama, K. Hosomi, H. Hashimoto, T. Shimamura, ^{1}H NMR spectra of the all-trans, 7-*cis*, 9-*cis*, 13-*cis* and 15-*cis* isomers of β-carotene: elongation of the double bond and shortening of the single bond toward the center of the conjugated chain as revealed by vicinal coupling constants, J. Mol. Struct. 193 (1989) 185.
[10] H. El-Qualja, D. Perrin, R. Martin, Kinetic study of the thermal oxidation of all-trans-beta-carotene and evidence for its antioxygen properties, New J. Chem. 19 (1995) 863.
[11] S.A. Everett, S.C. Kundu, S. Maddix, R.L. Wilson, Mechanisms of free radical scavenging by the nutritional antioxidant β-carotene, Biochem. Soc. Trans. (1995) 230.
[12] A. Schieber, R. Carle, Occurrence of carotenoid *cis*-isomers in food: Technological, analytical, and nutritional implications, Trends Food Sci. Technol. 16 (2005) 416.
[13] R.J. Bushway, A.M. Wilson, Determination of alpha- and beta-carotene in fruit and vegetables by high performance liquid chromatography, Can. Inst. Food. Sci. Technol. 15 (1982) 165.
[14] B.H. Chen, T.M. Chen, J.T. Chien, Kinetic model for studying the isomerization of alpha- and beta-carotene during heating and illumination, J. Agric. Food Chem. 42 (1994) 2391.
[15] B.H. Chen, H.Y. Peng, T.M. Chen, Changes of carotenoids, color, and vitamin A contents during processing of carrot juice, J. Agric. Food Chem. 43 (1995) 1912.
[16] F. Khachik, G.R. Beecher, N.F. Whittaker, Separation, identification, and quantification of the major carotenoid and chlorophyll constituents in extracts of several green vegetables by liquid chromatography, J. Agric. Food Chem. 34 (1986) 603.
[17] T. Noguchi, H. Hayashi, M. Tasumi, G.H. Atkinson, Solvent effects on the a_g C=C stretching mode in the 2^1Ag-excited state of β-carotene and two derivatives: picosecond time-resolved resonance Raman spectroscopy, J. Phys. Chem. 95 (1991) 3167.
[18] I. Saguy, M. Goldman, J. Karel, Prediction of beta-carotene decolorization under static and dynamic conditions of reduced oxygen environment, J. Food Sci. 50 (1985) 526.
[19] K.J. Yeum, R.M. Russell, Carotenoid bioavailability and bioconversion, Annu. Rev. Nutr. 22 (2002) 483.
[20] J.J.M. Castenmiller, C.E. West, Bioavailability and bioconversion of carotenoids, Annu. Rev. Nutr. 18 (1998) 19.
[21] M.C. Costa, R.A. Johnstone, D. Whittaker, Catalysis of gas and liquid phase ionic and radical rearrangements of alpha- and beta-pinene by metal(IV) phosphate polymers, J. Mol. Catal. A Chem. 104 (1996) 251.
[22] K.J. Crowley, A photochemical synthesis of beta-pinene, Proc. Chem. Soc. 89 (1962) 245.
[23] K.J. Crowley, Photoisomerizations. VI. Cyclobutene formation and diene migration in simple 1,3-dienes, Tetrahedron 21 (1965) 1001.
[24] W.G. Dauben, R.L. Cargill, R.M. Coates, J. Saltiel, The direct and sensitized irradiation of acyclic dienes, J. Am. Chem. Soc. 88 (1966) 2742.
[25] M. Ghandi, A. Rahimi, G. Mashayekhi, Triplet photosensitization of myrcene and some dienes within zeolite Y through heavy atom effect, J. Photochem. Photobiol. A Chem. 181 (2006) 56.
[26] R.S.H. Liu, G.S. Hammond, Photosensitized internal addition of dienes to olefins, J. Am. Chem. Soc. 89 (1967) 4936.
[27] A. Stolle, W. Bonrath, B. Ondruschka, Kinetic and mechanistic aspects of myrcene production via thermal-induced beta-pinene rearrangement, J. Anal. Appl. Pyrol. 83 (2008) 26.
[28] A. Andrzejewska, L. Lapinski, I. Reva, R. Fausto, Matrix isolation FTIR and molecular orbital study of E and Z acetaldoxime monomers, Phys. Chem. Chem. Phys. 4 (2002) 3289.
[29] M.J. Frisch, G.W. Trucks, H.B. Schlegel, G.E. Scuseria, M.A. Robb, J.R. Cheeseman, J.A. Montgomery Jr., T. Vreven, K.N. Kudin, J.C. Burant, N.J. Millam, S.S. Iyengar, J. Tomasi, V. Barone, B. Mennucci, M. Cossi, G. Scalmani, N. Rega, G.A. Petersson, H. Nakatsuji, M. Hada, M. Ehara, K. Toyota, R. Fukuda, J. Hasegawa, M. Ishida, T. Nakajima, Y. Honda, O. Kitao, H. Nakai, M. Klene, X. Li, J.E. Knox, H.P. Hratchian, J.B. Cross, V. Bakken, C. Adamo, J. Jaramillo, R. Gomperts, R.E. Stratmann, O. Yazyev, A.J. Austin, R. Cammi, C. Pomelli, J.W. Ochterski, P.Y. Ayala, K. Morokuma, G.A. Voth, P. Salvador, J.J. Dannenberg, V.G. Zakrzewski, S. Dapprich, A.D. Daniels, M.C. Strain, O. Farkas, D.K. Malick, A.D. Rabuck, K. Raghavachari, J.B. Foresman, J.V. Ortiz, Q. Cui, A.G. Baboul, S. Clifford, J. Cioslowski, B.B. Stefanov, G. Liu, A. Liashenko, P. Piskorz, I. Komaromi, R.L. Martin, D.J. Fox, T. Keith, M.A. Al-Laham, C.Y. Peng, A. Nanayakkara, M. Challacombe, P.M.W. Gill, B. Johnson, W. Chen, M.W. Wong, C. Gonzalez, J.A. Pople, GAUSSIAN 03, Revision E. 01, Gaussian, Inc., Wallingford, CT, 2004.
[30] M.J. Frisch, G.W. Trucks, H.B. Schlegel, G.E. Scuseria, M.A. Robb, J.R. Cheeseman, G. Scalmani, V. Barone, B. Mennucci, G.A. Petersson, H. Nakatsuji, M. Caricato, X. Li, H.P. Hratchian, A.F. Izmaylov, J. Bloino, G. Zheng, J.L. Sonnenberg, M. Hada, M. Ehara, K. Toyota, R. Fukuda, J. Hasegawa, M. Ishida, T. Nakajima, Y. Honda, O. Kitao, H. Nakai, T. Vreven, J.A. Montgomery Jr., J.E. Peralta, F. Ogliaro, M. Bearpark, J.J. Heyd, E. Brothers, K.N. Kudin, V.N. Staroverov, R. Kobayashi, J. Normand, K. Raghavachari, A. Rendell, J.C. Burant, S.S. Iyengar, J. Tomasi, M. Cossi, N. Rega, N.J. Millam, M. Klene, J.E. Knox, J.B. Cross, V. Bakken, C. Adamo, J. Jaramillo, R. Gomperts, R.E. Stratmann, O. Yazyev, A.J. Austin, R. Cammi, C. Pomelli, J.W. Ochterski, R.L. Martin, K. Morokuma, V.G. Zakrzewski, G.A. Voth, P. Salvador, J.J. Dannenberg, S. Dapprich, A.D. Daniels, Ö. Farkas, J.B. Foresman, J.V. Ortiz, J. Cioslowski, D.J. Fox, GAUSSIAN 09, Revision A1, Gaussian, Inc, Wallingford, CT, 2009.
[31] A.D. Becke, Density-functional thermochemistry. III. The role of exact exchange, J. Chem. Phys. 98 (1993) 5648.

[32] C. Lee, W. Yang, R.G. Parr, Development of the Colle–Salvetti correlation-energy formula into a functional of the electron density, Phys. Rev. B 37 (1988) 785.
[33] C. Peng, P.Y. Ayala, H.B. Schlegel, M.J. Frish, Using redundant internal coordinates to optimize equilibrium geometries and transition states, J. Comput. Chem. 17 (1996) 49.
[34] C. Peng, H.B. Schlegel, Combining synchronous transit and quasi-Newton methods to find transition states, Israel J. Chem. 33 (1993) 449.
[35] R. Bauernschmitt, R. Ahlrichs, Treatment of electronic excitations within the adiabatic approximation of time dependent density functional theory, Chem. Phys. Lett. 256 (1996) 454.
[36] M.E. Casida, C. Jamorski, K.C. Casida, D.R. Salahub, Molecular excitation energies to high-lying bound states from time-dependent density-functional response theory: characterization and correction of the time-dependent local density approximation ionization threshold, J. Chem. Phys. 108 (1998) 4439.
[37] K.M. Marzec, I. Reva, R. Fausto, K. Malek, L.M. Proniewicz, Conformational space and photochemistry of alpha-terpinene, J. Phys. Chem. A 114 (2010) 5526.
[38] S. Breda, I. Reva, R. Fausto, Molecular structure and vibrational spectra of 2(5H)-furanone and 2(5H)-thiophenone isolated in low temperature inert matrix, J. Mol. Struct. 887 (2008) 75.
[39] A. Kaczor, I.D. Reva, L.M. Proniewicz, R. Fausto, Importance of entropy in the conformational equilibrium of phenylalanine: a matrix-isolation infrared spectroscopy and density functional theory study, J. Phys. Chem. A 110 (2006) 2360.
[40] A. Kaczor, I.D. Reva, L.M. Proniewicz, R. Fausto, Matrix-isolated monomeric tryptophan: Electrostatic interactions as nontrivial factors stabilizing conformers, J. Phys. Chem. A 111 (2007) 2957.
[41] P. Pulay, G. Fogarasi, F. Pang, J.E. Boggs, Systematic ab initio gradient calculation of molecular geometries, force constants, and dipole moment derivatives, J. Am. Chem. Soc. (1979) 2550.
[42] J.M.L. Martin, C. Van Alsenoy, GAR2PED, University of Antwerp, 1995.
[43] S. Saha, F. Wang, C.T. Falzon, M.J. Brunger, Coexistence of 1,3-butadiene conformers in ionization energies and Dyson orbitals, J. Chem. Phys. 123 (2005) 124315.
[44] L.A. Carreira, Determination of the torsional potential function of 1,3-butadiene, J. Chem. Phys. 62 (1975) 3851.
[45] R. Engeln, D. Consalvo, J. Reuss, Evidence for a gauche minor conformer of 1,3-butadiene, Chem. Phys. 160 (1992) 427.
[46] A.J. Lopes Jesus, M.T.S. Rosado, I. Reva, R. Fausto, M.E.S. Eusebio, J.S. Redinha, Structure of isolated 1,4-butanediol: combination of MP2 calculations, NBO analysis, and matrix-isolation infrared spectroscopy, J. Phys. Chem. A 112 (2008) 4669.
[47] A.J. Lopes Jesus, M.T.S. Rosado, I. Reva, R. Fausto, M.E.S. Eusebio, J.S. Redinha, Conformational study of monomeric 2,3-butanediols by matrix-isolation infrared spectroscopy and DFT calculations, J. Phys. Chem. A 110 (2006) 4169.
[48] I.D. Reva, A.J. Lopes Jesus, M.T.S. Rosado, R. Fausto, M.E.S. Eusebio, J.S. Redinha, Stepwise conformational cooling towards a single isomeric state in the four internal rotors system 1,2-butanediol, Phys. Chem. Chem. Phys. 8 (2006) 5339.
[49] M.T.S. Rosado, A.J. Lopes Jesus, I.D. Reva, R. Fausto, J.S. Redinha, Conformational cooling dynamics in matrix-isolated 1,3-butanediol, J. Phys. Chem. A 113 (2009) 7499.
[50] R. Srinivasan, A simple synthesis of bicyclo [1.1.0]butane and its relation to the internal conversion of electronic energy in 1,3-butadiene, J. Am. Chem. Soc. 85 (1963) 4045.
[51] M.E. Squillacote, R.S. Sheridan, O.L. Chapman, F.A.L. Anet, Planar s-cis-1,3-butadiene, J. Am. Chem. Soc. 101 (1979) 3657.
[52] W. Fuss, W.E. Schmid, S.A. Trushin, Ultrafast electronic relaxation of s-*trans*-butadiene, Chem. Phys. Lett. 342 (2001) 91.
[53] R.P. Krawczyk, K. Malsch, G. Hohlneicher, R.C. Gillen, W. Domcke, 1 B-1(u)-2(1)A(g) conical intersection in trans-butadiene: ultrafast dynamics and optical spectra, Chem. Phys. Lett. 320 (2000) 535.
[54] R.M. Gavin, S. Risemberg, S.A. Rice, G.H. Atkinson, Spectroscopic properties of polyenes I. The lowest energy allowed singlet–singlet transition for *cis*- and *trans*-1,3,5-hexatriene, J. Chem. Phys. 58 (1973) 3160.
[55] P. Celani, F. Bernardi, M. Olivucci, M.A. Robb, Excited-sate reaction pathways for s-*cis* buta-1,3-diene, J. Chem. Phys. 102 (1995) 5733.
[56] M. Garavelli, F. Bernardi, M. Olivucci, M.J. Bearpark, S. Klein, M.A. Robb, Product distribution in the photolysis of s-*cis* butadiene: a dynamics simulation, J. Phys. Chem. A 105 (2001) 11496.
[57] M. Olivucci, F. Bernardi, S. Ottani, M.A. Robb, Substituent effect in buta-1,3-diene photochemistry: a CAS-SCF Study of 2,3-dimethylbutadiene and 2-cyanobutadiene excited-state reaction paths, J. Am. Chem. Soc. 116 (1994) 2034.
[58] M. Olivucci, I.N. Ragazos, F. Bernardi, M.A. Robb, A conical intersection mechanism for the photochemistry of butadiene. A MC-SCF study, J. Am. Chem. Soc. 115 (1993) 3710.
[59] R.D. Walker, J.E. Hawkins, The ultraviolet absorption spectra of some terpene hydrocarbons, J. Am. Chem. Soc. 74 (1952) 4209.
[60] S. Breda, I. Reva, L. Lapinski, R. Fausto, Matrix isolation FTIR and theoretical study of alpha-pyrone photochemistry, Phys. Chem. Chem. Phys. 6 (2004) 929.